Contents lists available at ScienceDirect

NeuroImage: Clinical

Spatial distributions of cholinergic impairment and neuronal hypometabolism differ in MCI due to AD

Nils Richter[a,b,c,*], Nils Nellessen[a,b], Julian Dronse[a,b], Kim Dillen[b], Heidi I.L. Jacobs[b,d,e,f], Karl-Josef Langen[g], Markus Dietlein[h], Lutz Kracht[c,h], Bernd Neumaier[i,j], Gereon R. Fink[a,b], Juraj Kukolja[b,k,1], Oezguer A. Onur[a,b,1]

[a] *Department of Neurology, University Hospital Cologne, 50937 Cologne, Germany*
[b] *Cognitive Neuroscience, Institute of Neuroscience and Medicine (INM-3), Research Center Jülich, 52425 Jülich, Germany*
[c] *Max-Planck-Institute for Metabolism Research, 50937 Cologne, Germany*
[d] *Division of Nuclear Medicine and Molecular Imaging, Department of Radiology, Massachusetts General Hospital/Harvard Medical School, Boston, MA, United States of America*
[e] *The Athinoula A. Martinos Center for Biomedical Imaging, Department of Radiology, Massachusetts General Hospital/Harvard Medical School, Boston, MA, United States of America*
[f] *Faculty of Health, Medicine and Life Sciences, School for Mental Health and Neuroscience, Alzheimer Centre Limburg, Maastricht University, Maastricht, the Netherlands*
[g] *Medical Imaging Physics (INM-4), Institute of Neuroscience and Medicine (INM-4), Research Center Jülich, 52425 Jülich, Germany*
[h] *Department of Nuclear Medicine, University Hospital Cologne, 50937 Cologne, Germany*
[i] *Institute for Radiochemistry and Experimental Molecular Imaging, University Hospital Cologne, 50937 Cologne, Germany*
[j] *Nuclear Chemistry, Institute of Neuroscience and Medicine (INM-5), Research Center Jülich, 52425 Jülich, Germany*
[k] *Department of Neurology and Neurophysiology, Helios University Hospital Wuppertal, 42283 Wuppertal, Germany*

ARTICLE INFO

ABSTRACT

Elucidating the relationship between neuronal metabolism and the integrity of the cholinergic system is prerequisite for a profound understanding of cholinergic dysfunction in Alzheimer's disease.

The cholinergic system can be investigated specifically using positron emission tomography (PET) with $[^{11}C]$ *N*-methyl-4-piperidyl-acetate (MP4A), while neuronal metabolism is often assessed with 2-deoxy-2-$[^{18}F]$fluoro-D-glucose-(FDG) PET. We hypothesised a close correlation between MP4A-perfusion and FDG-uptake, permitting inferences about metabolism from MP4A-perfusion, and investigated the patterns of neuronal hypometabolism and cholinergic impairment in non-demented AD patients.

MP4A-PET was performed in 18 cognitively normal adults and 19 patients with mild cognitive impairment (MCI) and positive AD biomarkers. In nine patients with additional FDG-PET, the sum images of every combination of consecutive early MP4A-frames were correlated with FDG-scans to determine the optimal time window for assessing MP4A-perfusion. Acetylcholinesterase (AChE) activity was estimated using a 3-compartmental model. Group comparisons of MP4A-perfusion and AChE-activity were performed using the entire sample.

The highest correlation between MP4A-perfusion and FDG-uptake across the cerebral cortex was observed 60–450 s after injection (r = 0.867). The patterns of hypometabolism (FDG-PET) and hypoperfusion (MP4A-PET) in MCI covered areas known to be hypometabolic early in AD, while AChE activity was mainly reduced in the lateral temporal cortex and the occipital lobe, sparing posterior midline structures.

Data indicate that patterns of cholinergic impairment and neuronal hypometabolism differ significantly at the stage of MCI in AD, implying distinct underlying pathologies, and suggesting potential predictors of the response to cholinergic pharmacotherapy.

1. Introduction

Currently, there is renewed interest in the role of the cholinergic system in physiological aging and Alzheimer's disease (AD) (Bohnen et al., 2018; Grothe et al., 2016; Hampel et al., 2018a; Richter et al., 2018; Schmitz et al., 2018; Schmitz et al., 2016), arguably influenced

by recent challenges in the development of anti-amyloid- and anti-tau-treatments (Cummings et al., 2014; Hampel et al., 2018b). To date, the only effective medical treatments for dementia due to AD target the cholinergic and glutamatergic neurotransmission (Cummings et al., 2014). Significant advances have recently been made concerning the imaging of the cholinergic system. For positron emission tomography (PET), the [^{18}F]-based tracers [^{18}F]-fluoroethoxybenzovesamicol (FEOBV), which binds to the presynaptic vesicular acetylcholine transporter (Aghourian et al., 2017; Schmitz et al., 2018), and [^{18}F]-flubatine, a ligand of α4β2 nicotinic acetylcholine receptors (Sabri et al., 2018), were developed for use in humans. A multimodal pharmacological imaging study using the acetylcholinesterase-(AChE)-tracer [^{11}C]-N-methyl-4-piperidyl acetate (MP4A) revealed that the imaging of the cholinergic system allows identifying patients who will benefit from cholinergic stimulation before showing dementia (Richter et al., 2018). The tracers used in the studies mentioned above were designed to provide specific information about the cholinergic system (Aghourian et al., 2017; Namba et al., 1999), rather than regional hypometabolism, which in turn is thought to reflect the extent of neuronal injury (Albert et al., 2011). Regional hypometabolism is routinely assessed by 2-deoxy-2-[^{18}F]fluoro-D-glucose ([^{18}F]-FDG)-PET (Teipel et al., 2015). As for most PET tracers, the distribution of MP4A during the first minutes after intravenous injection largely depends on cerebral perfusion (Herholz et al., 2000), which – in turn – is closely linked to cerebral glucose metabolism (Paulson et al., 2010). Consistently, for a number of PET-tracers of amyloid- and tau-pathology scans acquired early after injection highly correlated with [^{18}F]-FDG-PET scans of the same individual (Daerr et al., 2017; Forsberg et al., 2012; Hammes et al., 2017; Hsiao et al., 2012; Rodriguez-Vieitez et al., 2017; Rostomian et al., 2011). Evidence from patients with dementia due to AD suggests that a similar approach may be feasible using MP4A (Herholz et al., 2000).

AD pathology develops years before the patients show symptoms of dementia (Bateman et al., 2012; Jack et al., 2010; Knopman et al., 2012). Since it is widely assumed that treatment may be more effective before neurodegeneration has proceeded, the focus of current research of pharmacological treatment of AD has shifted to the earliest stages of the disease (Sperling et al., 2011). We here studied patients with positive cerebrospinal fluid-based biomarkers, suggesting AD, at the stage of mild cognitive impairment (MCI), characterised by relatively subtle, but objectifiable neuropsychological deficits despite unimpaired activities of daily living. We hypothesised that the radiotracer MP4A, designed to characterise the cholinergic system, could additionally provide information on neuronal metabolism that is routinely assessed by FDG. Specifically, we hypothesised (1) that MP4A-perfusion during the first ten minutes after injection is highly correlated with FDG-uptake, especially in areas with glucose hypometabolism, and (2) that patterns of hypometabolism and reduced AChE activity at this disease stage would be distinctly different.

2. Methods

2.1. Participants

Twenty patients diagnosed with MCI (11 male, 9 female, aged 54 to 80, mean 68.8 ± 6.8 years), without neurological or psychiatric co-morbidities and positive cerebrospinal fluid-based biomarkers of AD pathology and signs of neuronal injury, were recruited as part of the study MACS (Memory, Aging and the Cholinergic System, EudraCT No. 2008–008896-32) as previously described in detail (Richter et al., 2018; Richter et al., 2017). In brief, the ethics committee of the medical faculty of the University of Cologne, as well as local and federal authorities, had approved the study. All participants provided written informed consent before the study. One patient withdrew the consent during the study. Twenty-two cognitively normal older adults (14 male, 8 female, aged 53 to 80, mean 66.6 ± 7.1 years) without a history of a

neurological or psychiatric disease and cholinergic, anticholinergic or other psychoactive drugs were recruited from the community as controls. Five participants were not eligible for further analyses due to an incidental pathological finding ($n = 1$; severe cerebral atrophy), severe dental metal artefacts in MRI (n = 2), PET acquisition failure due to technical issues (n = 1), and withdrawn consent (n = 1). Nine patients had additionally received FDG-PET during the routine clinical workup. Thus, MP4A data of 18 controls and 19 MCI patients entered the analyses, and FDG- and MP4A-scans were available from a subsample of 9 patients. To assess the pattern of glucose hypometabolism, the nine patients that had also received an FDG-PET were compared to FDG-scans from twelve cognitively normal older healthy adults (8 male, 4 female, aged 51 to 79, mean 64.5 ± 9.5 years) without history of medical or psychiatric illness, who had received an FDG-PET scan at the MR-Brain-PET under the same conditions.

All participants underwent a physical and neurological examination by a neurologist and a comprehensive neuropsychological assessment consisting of the German version of the Mini-Mental State Exam (MMSE) (Kessler et al., 1990), Beck's Depression Inventory V (Schmitt et al., 2006), the Bayer Activities of Daily Living (Hindmarch et al., 1998), the Trail-Making-Test A and B (Berres et al., 2000), Brief Test of Attention (Schretlen et al., 1996), the Leistungsprüfsystem part 4 (logical thinking) (Horn, 1983), the Verbal Learning and Memory Test (VLMT; the German version of the Rey Auditory Learning Test (Helmstaedter et al., 2001)), and the Rey-Osterrieth Complex Figure Test (ROCF) (Rey, 1964). MCI was defined as performance > 1.5 standard deviations below the norm in the delayed recall of the VLMT, and > 24 points in the MMSE, as well as normal scores in tests of attention, logical thinking and activities of daily life.

2.2. Imaging acquisition

MP4A was synthesised as previously described (Haense et al., 2012; Herholz et al., 2000), with minor modifications, and 471.06 MBq (standard deviation 78.99 MBq) were injected intravenously as a bolus. MP4A-PET-scanning was performed immediately after tracer injection using an ECAT HRRT scanner (CPS Innovations, Knoxville TN, USA) using the protocol described by Haense et al. (2012). Participants had their eyes closed and ears unplugged in a dimly lit room with minimal background noise.

FDG scanning was performed using a 3 T MR-Brain-PET scanner (Siemens, Erlangen, Germany) consisting of a 3 T MR system MAGNE-TOM Trio with a custom built BrainPET insert in the bore of the magnet (Herzog et al., 2011). After intravenous injection of 200 MBq FDG, patients lay supine in the MR scanner while structural and functional MRI scans were acquired. During this time patients were instructed to keep their eyes open to avoid falling asleep. They wore earplugs to reduce MR-scanner noise. FDG-scanning was performed during minutes 30–60 after injection and reconstructed with OSEM in 5-minute frames. After filtering with a Gaussian kernel of 3 mm FWHM, frames were realigned using PMOD Version 3.4 (PMOD Technologies Ltd., Zurich, Switzerland) and summed. The average time delay between FDG- and MP4A scanning was 73.8 days (standard deviation: 40.5 days). High-resolution T1-weighted images (MDEFT3D; repetition time (TR) 1930 ms; inversion time (TI) 650 ms; echo time (TE) 5.8 ms; flip angle 18°; 128 sagittal slices; resolution 1.0 × 1.0 × 1.25 mm^3) were acquired using a 3 T Trio scanner (Siemens, Erlangen, Germany) with a 32-channel coil.

2.3. PET processing

Basic image arithmetics, realignment and co-registration of images were performed employing different modules of the FSL software package (FMRIB's Software Library, Version 5.0, http://www.fmrib.ox.ac.uk/fsl) as follows. For the nine patients who had both an MP4A- and an FDG-PET scan, the first ten frames of each MP4A-scan, covering

0–600 s, were realigned with MCFLIRT (Jenkinson et al., 2002) and summed in all possible combinations of consecutive frames. The resulting early MP4A-windows (from here on referred to as MP4A-perfusion images) were rigidly co-registered to the participant's FDG-scan, which had previously been co-registered to the corresponding high-resolution T1-image using FLIRT (Jenkinson and Smith, 2001). A nonlinear spatial normalization of the T1-image to MNI-space was performed using the CAT12 toolbox (Computational AnatomyToolbox 12, http://www.neuro.uni-jena.de/cat/) implemented in SPM12 (www.fil.ion.ucl.ac.uk/spm/software/spm12) and resampled to an isotropic resolution of 2 mm. The deformation fields computed in this process were applied to the co-registered MP4A-perfusion images, thereby normalising these to MNI-space. MP4A-perfusion images were smoothed with a Gaussian kernel 11 mm FWHM and FDG- images with a Gaussian kernel of 8 mm FWHM for an equal resultant smoothness.

AChE activity was assessed by quantifying the hydrolysis rate k_3 of MP4A at the voxel level. Images were processed as follows: (1) Rigid-body co-registration of the sum of the first 10 min of the PET-scan to the T1-image; (2) rigid-body co-registration of all consecutive frames to the co-registered first 10-minute frame; (3) filtering of all individual frames with a Gaussian kernel (12 mm FWHM) with restriction of the kernel to avoid smoothing across high gradients of signal contrast; (4) segmentation (segmentations were visually assessed and edited as necessary) and parcellation of the T1-image using FreeSurfer 5.0.0 (Dale et al., 1999; Fischl et al., 2002, 2004); (5) extraction of the kinetic reference curve from a putaminal region of interest (ROI) defined by use of the segmented and parcellated T1-image; (6) computation of k_3 of MP4A at the voxel level (Herholz et al., 2000; Zundorf et al., 2002) as implemented in the software package VINCI (version 4.20, Max-Planck Institute for Neurological Research, Cologne, Germany); (7) application of the nonlinear normalization parameters obtained in the VBM analysis to the parametric k_3-images resulting from the previous step.

2.4. Statistical analyses

For each of the nine patients that had undergone FDG- and MP4A-PET scanning, Pearson correlations between the two modalities were computed at the voxel level for each MP4A-perfusion image using an in-house script in the software R (https://cran.r-project.org/). To average the intra-subject correlation coefficients across patients, their Fisher-Z-transformations were computed and averaged, and the resulting values were transformed back to r values (Hammes et al., 2017). Since cerebral hypometabolism in AD is primarily observed in the cortex (Herholz, 1995; Minoshima et al., 1997), the perfusion window showing the highest correlation with FDG-uptake across the cerebral cortex was chosen as the "optimal window".

In this subsample of nine patients that had undergone FDG- and MP4A-PET scanning, across-subject correlation coefficients between MP4A-perfusion images of this optimal window and FDG images were computed voxel-wise with FSL *randomise* using two types of SUVR image for each modality: (1) using the putamen, which also served as reference region for k_3 estimation, and (2) using the whole brain as reference regions. Regions of interest were defined using the Harvard-Oxford (Makris et al., 2006) and the MNI anatomical atlases (Mazziotta et al., 2001), implemented in FSL.

To assess the spatial patterns of glucose hypometabolism, hypoperfusion and reduced AChE activity in MCI patients, 2-sample t-tests against age-matched controls were computed at the voxel level using non-parametric permutation testing as implemented in FSL *randomise* (Nichols and Holmes, 2002; Winkler et al., 2014). For the comparisons of perfusion and AChE activity, all 18 controls and 19 patients entered the analyses. Perfusion images with the whole brain as reference region were used in the voxel-wise comparisons. To assess the pattern of glucose hypometabolism, the nine patients who had also received an FDG-PET were compared to FDG-scans from a separate sample of twelve cognitively normal older healthy adults, as described above.

Table 1
Number of participants.

Test	Controls [n]	Patients [n]
Intra-subject correlation between FDG-uptake and MP4A-perfusion		9[a]
Across subject correlation between FDG-uptake and MP4A-perfusion		9[a]
Group comparison of FDG-uptake	12	9[a]
Group comparison of MP4A-perfusion	18	19
Group comparison of k_3 of MP4A	18	19

[a] Subset of the 19 patients in the group comparisons.

Resulting statistical maps were family-wise error (FWE) corrected using threshold-free cluster enhancement (Smith and Nichols, 2009) and thresholded at p < .05 and a cluster size of ≥100 voxels. The group sizes for the statistical comparisons are summarised in Table 1.

3. Results

3.1. Correlations between MP4A-perfusion and FDG images

As illustrated in Fig. 1, there was a high degree of similarity between MP4A-perfusion and the corresponding FDG-uptake images at the level of the individual patient. Across the cerebral cortex, the strongest correlation between FDG-uptake and perfusion was observed during the time from 90 s to 450 s post injection (r = 0.867). However, the correlation coefficients across all time-windows covering more than the first 60 s after injection were quite similar, at least 0.775 and for the most above 0.85 (Table 2).

Across patients, the highest correlations between FDG-uptake and MP4A-perfusion during the optimal time window (90–450 s after injection), with the whole brain as reference region, were observed in areas typically showing FDG-hypometabolism in early AD (Herholz, 1995; Minoshima et al., 1997), namely in the parietal lobe (r = 0.768), and to a lesser degree in the temporal and frontal lobes (Fig. 2 and Table 3). Generally, correlations were much stronger, especially in the cortex, when using the whole brain as the reference region for the SUVR images instead of the putamen (Table 3).

3.2. Group comparisons

FDG uptake was significantly lower in patients compared to controls, especially in posterior midline structures (precuneus and posterior cingulate cortex (PCC)) with a maximum in the precuneus, but also the angular gyrus bilaterally and, to a lesser degree in the posterior part of
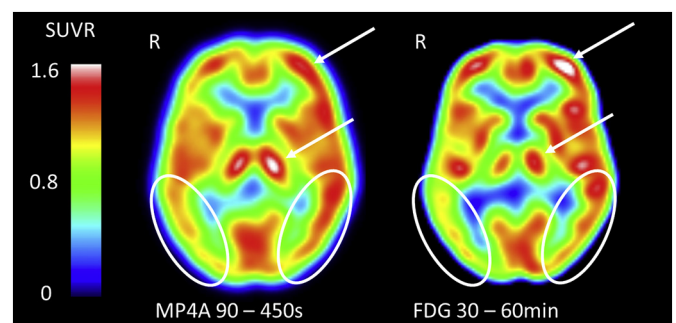

Fig. 1. Representative axial slices from a patient with MCI due to AD, illustrating the similarity in the patterns of glucose metabolism (FDG-PET, 30–60 min) and perfusion (MP4A-PET 90–450 s). Ellipses highlight the similar pattern of parietal hypometabolism and decreased perfusion (right more than left side). Arrows highlight the different relationships between cortical and subcortical signals in perfusion and FDG-images.

Table 2
Voxel-wise intra-subject correlation coefficients between FDG-PET (30–60 min) and every early MP4A-PET time window (i.e. start times 0–450 s and end times 30–600 s) pooled across the cerebral cortex in patients with MCI due to AD ($n = 9$). The highest correlation coefficient was observed for the window from 90–450 s, as highlighted in bold font.

End	30 s	60 s	90 s	120 s	150 s	180 s	240 s	300 s	450 s	600 s
Start										
0 s	−0.0918	0.6707	0.7757	0.8137	0.8317	0.8438	0.8481	0.8556	0.8570	0.8575
30 s		0.7139	0.7940	0.8224	0.8370	0.8477	0.8510	0.8582	0.8603	0.8594
60 s			0.8158	0.8399	0.8535	0.8572	0.8621	0.8635	0.8662	0.8657
90 s				0.8268	0.8514	0.8549	0.8598	0.8643	**0.8670**	0.8661
120 s					0.8387	0.8518	0.8601	0.8658	0.8667	0.8656
150 s						0.8334	0.8539	0.8641	0.8654	0.8639
180 s							0.8452	0.8601	0.8636	0.8605
240 s								0.8469	0.8568	0.8548
300 s									0.8454	0.8436
450 s										0.8223

the left inferior temporal gyrus (Fig. 3a, Table 4). The pattern of MP4A-perfusion-reduction was similar to that of FDG-hypometabolism, with the most significant differences in the PCC and the angular gyrus bilaterally (Fig. 3b, Table 4). Interestingly, MP4A-perfusion was higher in patients than in controls in the central region, with maxima in the left precentral gyrus, the right postcentral gyrus and the right cerebellum (Fig. 3c, Table 4). The pattern of lower levels of cortical AChE activity was distinctly different from the group difference in perfusion and glucose metabolism (Fig. 3d). In patients, AChE activity was significantly lower in the lateral temporal cortex and the occipital cortex (for local maxima, please see Table 4). The PCC and the precuneus exhibited the most significant group differences in the other modalities but showed no significant group difference in AChE activity.

4. Discussion

We here demonstrate that perfusion images generated from MP4A-PET provide distinct and valuable information independent of AChE activity images. MP4A perfusion images were highly similar to the pattern of neuronal hypometabolism revealed by FDG-PET. Importantly, this pattern was distinctly different from the cholinergic changes at the stage of MCI in AD. While glucose hypometabolism and hypoperfusion were constrained to posterior midline structures and the temporo-parietal junction, AChE activity was lower in patients throughout the lateral temporal, parietal and occipital cortices.

4.1. Spatial heterogeneity of cholinergic impairment and neuronal hypometabolism

In stark contrast to the similar patterns of decreased perfusion and glucose hypometabolism in MCI, with maxima in the precuneus and PCC as well as the temporoparietal junction, the pattern of lower AChE activity was distinctly different. In line with the literature, patients' AChE activity was significantly decreased in lateral temporal, parietal

Table 3
Regional across subject correlations between glucose metabolism (FDG-PET, 30–60 min) and perfusion (MP4A-PET 90–450 s) in patients with MCI due to AD ($n = 9$).

	Whole Brain reference	Putamen reference
Region of interest	correlation coefficient	correlation coefficient
Whole cortex	0.628	0.483
Parietal cortex	0.768	0.679
Temporal cortex	0.675	0.528
Frontal cortex	0.670	0.441
Occipital cortex	0.449	0.327
Basal ganglia	0.314	0.373
Thalamus	0.358	0.372
Brain Stem	0.355	0.197

and occipital cortices and to a lesser degree in the frontal cortex, sparing the posterior midline structures most severely affected in the other modalities (Haense et al., 2012; Richter et al., 2018; Richter et al., 2017). This pattern fits the caudo-rostral gradient of neuronal loss in the Nucleus basalis of Meynert (NbM), the origin of most cholinergic input to the neocortex. The most caudally situated part of the NbM providing cholinergic input to the superior temporal gyrus and the temporal pole is affected first, followed by neuronal populations projecting to the convexities of the cortex and the entire occipital cortex. The most rostral part of the NbM providing input to the posterior midline structures and the medial frontal lobe is affected later in the disease process (Liu et al., 2015). Hence, in AD, the decrease of cortical AChE activity is expected to begin in lateral temporal areas and to spread across the convexities and affect the midline structures at later disease stages. A recent PET study reported a reduction of the vesicular acetylcholine transporter in lateral temporal cortices and inferior parietal areas in dementia due to AD. However, the authors also reported significant reductions of FEOBV uptake in posterior midline structures (Aghourian et al., 2017). This discrepancy to our findings is best
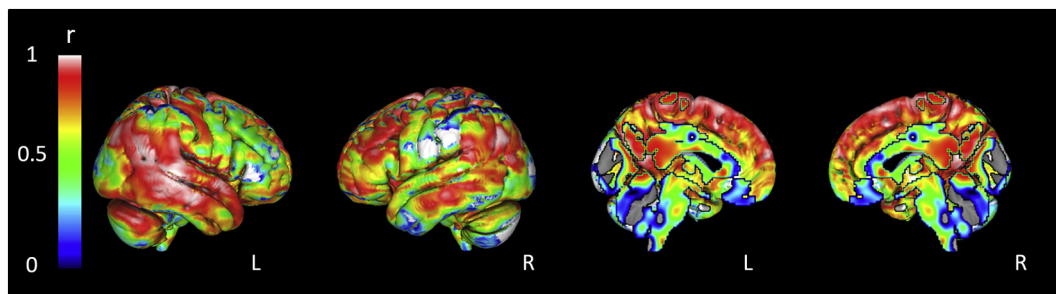

Fig. 2. Spatial distribution of the voxel-wise across subject correlation between glucose metabolism (FDG-PET, 30–60 min) and perfusion (MP4A-PET 90–450 s) in patients with MCI due to AD (n = 9).
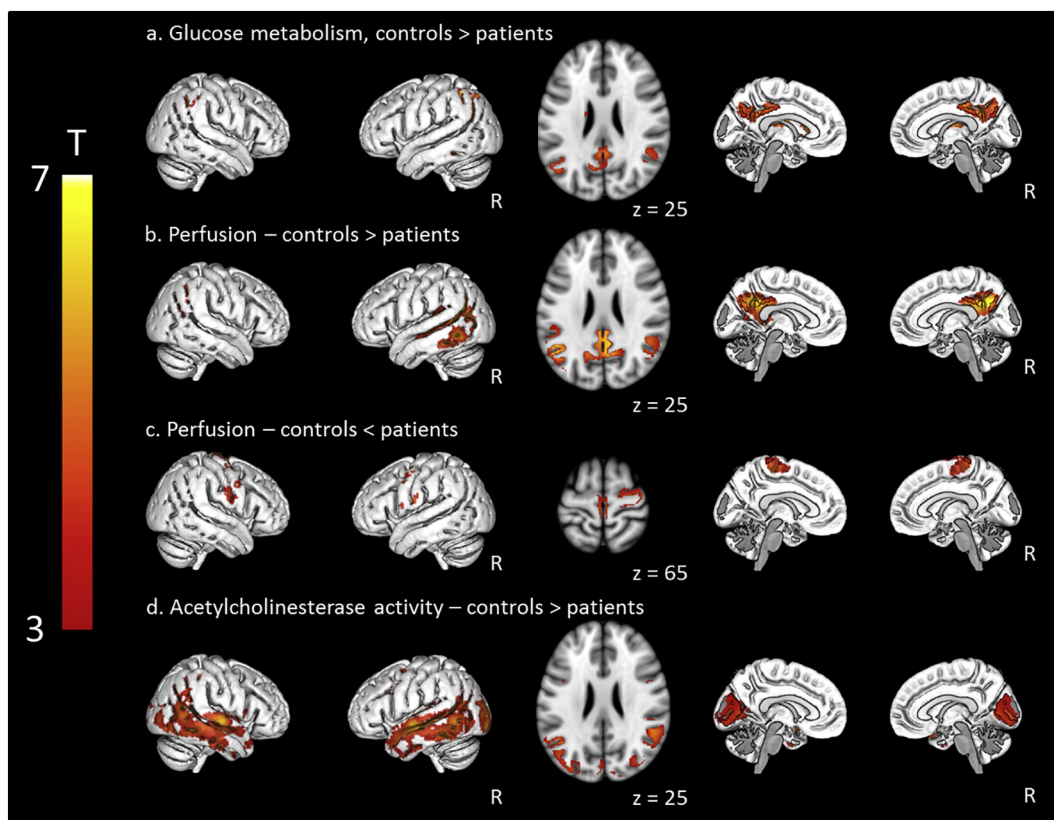
Fig. 3. Metabolic changes in MCI compared to age-matched controls. Voxel-wise T-tests comparing (a.) FDG-uptake (12 controls, 9 patients; 30–60 min p.i.), (b. and c.) MP4A-perfusion (18 controls, 19 patients; 90–450 s p.i.) and (d.) k_3 of MP4A (18 controls, 19 patients). All comparisons are significant at a threshold-free cluster enhancement FWE-corrected $p < .05$. z-values indicate the axial slice position (in MNI-coordinates).

Table 4
Group comparisons.

Voxels	T	x	y	z	Structure	Side
FDG: controls ($n = 12$) > MCI ($n = 9$)						
1416	6.8	−8	−66	32	Precuneus	L
1137	6.79	−46	−52	50	Angular gyrus	L
1025	6.63	44	−50	54	Angular gyrus	R
197	5.62	−58	−26	−22	Inferior temporal gyrus, posterior	L
Perfusion: controls ($n = 18$) > MCI ($n = 19$)						
Voxels	T	x	y	z	Structure	Side
7311	5.56	−46	−58	24	Angular gyrus	L
4834	5.02	46	−52	28	Angular gyrus	R
4203	5.57	−2	−50	32	PCC	L
Perfusion: controls ($n = 18$) < MCI ($n = 19$)						
Voxels	T	x	y	z	Structure	Side
1531	4.67	−6	−26	60	Precentral Gyrus	L
225	5.83	22	−50	−28	Cerebellum	R
101	4	64	−6	26	Postcentral Gyrus	R
Acetylcholinesterase activity: controls ($n = 18$) > MCI ($n = 19$)						
Voxels	T	x	y	z	Structure	Side
32,345	6.45	−60	−12	−6	Superior temporal gyrus	L
	6.02	−38	−82	10	Inferior lateral occipital cortex	L
	5.96	66	−14	0	Superior temporal gyrus	R
	5.25	48	−66	−10	Inferior lateral occipital cortex	R
	4.55	−36	12	32	Middle frontal gyrus	L
	4.34	42	−62	46	Superior lateral occipital cortex	R

explained by more widespread pathological changes at the stage of dementia than at the stage of MCI due to AD. In line with this explanation, AChE activity measured using MP4A has also been reported to be reduced in the posterior midline in manifest dementia due to AD (Herholz et al., 2000; Shinotoh et al., 2000).

While glucose hypometabolism and hypoperfusion are first observed in the posterior midline structures and spread to the lateral cortices in the course of the disease, the cholinergic deficit is first observed in lateral temporal areas and involves the precuneus and PCC at a later stage of the disease. These distinct spatial distributions of altered cerebral metabolism and AChE activity at the stage of MCI in our data and their distribution in dementia due to AD imply different spatio-temporal dynamics of neuronal injury and cholinergic impairment in early disease stages and a complex relationship to AD pathology. In early disease stages the effects of remote pathology dominate: Neuronal hypometabolism in the posterior midline is associated with hippocampal injury (Teipel et al., 2016), while cortical cholinergic impairment is attributable to AD pathology in the basal forebrain. At later disease stages local pathology seems to play a greater role (Aghourian et al., 2017; Teipel et al., 2016). Further investigations are warranted to determine if these two parameters or corresponding structural changes, i.e. the ratio between hippocampal and basal forebrain atrophy, may be used to predict the response to cholinergic pharmacotherapy in AD at the stage of MCI.

4.2. Correlations between MP4A perfusion and FDG-PET

A high degree of similarity between the MP4A-perfusion images and FDG-scans was noticeable already on visual inspection. The two PET-modalities were highly correlated within participants during all time windows after the first minute post injection, as in previous reports (Daerr et al., 2017; Hammes et al., 2017; Rodriguez-Vieitez et al., 2017; Rostomian et al., 2011; Tiepolt et al., 2016). The specific binding of MP4A did not have detrimental effects on perfusion images, even during the later part of the first ten minutes after injection.

Across patients, the closest correlation between perfusion and glucose metabolism was observed in the parietal cortex, followed by the

temporal and frontal cortex, while the occipital cortex showed the weakest correlation. The particularly close association between the two modalities in the temporoparietal cortices, known to show pronounced glucose hypometabolism in early AD (Herholz, 1995; Minoshima et al., 1997), is in line with previous reports (Hammes et al., 2017; Mielke et al., 1994). The high correlation between the two modalities is all the more striking in light of the delay between the two PET measurements (73.8 days on average), the use of two different PET scanners, and the fact that patients were only at the stage of MCI. The weakest correlations were observed in subcortical structures. This is likely due to the fact that across-subject correlations depend on local signal variance (cf. Hammes et al., 2017), and that signal variance in areas unaffected by disease - such as the basal ganglia - is typically low, resulting in weak correlations between perfusion and glucose metabolism. Low correlations observed in the occipital cortex are probably also attributable to the fact that occipital cortex is affected late in the course of the disease, or that patients had their eyes open during the acquisition of the FDG-PET and closed during MP4A-PET scanning.

ROI-wise correlation coefficients (Table 3) demonstrate a closer association between the two modalities when using the whole brain as the reference region instead of the putamen. While AChE activity is much higher in subcortical structures than in the cerebral cortex (Arai et al., 1984; Atack et al., 1987; Namba et al., 1999), this discrepancy likely results from the fact that the subcortico-cortical signal ratio is higher in perfusion than in glucose metabolism (cf. thalamic and cortical signal in Fig. 1), since similar phenomena have been observed using the non-cholinergic tracers $[^{15}O]$-H$_2$O (Wong et al., 2006) and $[^{18}F]$-AV-1451 (Hammes et al., 2017).

In MCI, glucose metabolism was significantly decreased in the precuneus and the angular gyrus bilaterally as well as the posterior part of the left inferior temporal gyrus. These structures have consistently been described as sites of glucose hypometabolism in MCI due to AD (Minoshima et al., 1997; Morbelli et al., 2017; Pagani et al., 2015). In contrast, perfusion was increased in the central region and the cerebellum in MCI (cf. Fig. 3c, Table 4), regions typically less affected in AD at this stage of the disease (Minoshima et al., 1995). This phenomenon has been reported when using the whole-brain signal to compute the SUVR (Hammes et al., 2017; Mielke et al., 1994). Since the whole-brain reference region also encompasses areas with decreased perfusion, leading to a smaller denominator in the ratio of the patient group, perfusion is overestimated in unaffected areas.

5. Conclusion

Spatial patterns of decreased AChE activity and hypometabolism in MCI differ significantly, suggesting a complex relationship to remote pathology at this stage of AD. Further studies are warranted to determine the utility of pathological changes in specific structures as predictors of responsiveness to cholinergic pharmacotherapy at the MCI stage.

Furthermore, the early acquisition windows of MP4A-PET are highly correlated with FDG-PET, revealing a substantial overlap of FDG hypometabolism and MP4A hypoperfusion. Complementary information about hypometabolism and cholinergic impairment can thus be obtained from a single PET examination, reducing the burden on study participants and patients, simplifying logistics in research and clinical settings.

Acknowledgements

Declarations of Competing Interest

None.

References

Aghourian, M., Legault-Denis, C., Soucy, J.P., Rosa-Neto, P., Gauthier, S., Kostikov, A., Gravel, P., Bédard, M.A., 2017. Quantification of brain cholinergic denervation in Alzheimer's disease using PET imaging with [^{18}F]-FEOBV. Mol. Psychiatry 22, 1531–1538.

Albert, M.S., DeKosky, S.T., Dickson, D., Dubois, B., Feldman, H.H., Fox, N.C., Gamst, A., Holtzman, D.M., Jagust, W.J., Petersen, R.C., Snyder, P.J., Carrillo, M.C., Thies, B., Phelps, C.H., 2011. The diagnosis of mild cognitive impairment due to Alzheimer's disease: recommendations from the National Institute on aging-Alzheimer's association workgroups on diagnostic guidelines for Alzheimer's disease. Alzheimers Dement. 7, 270–279.

Arai, H., Kosaka, K., Muramoto, O., Iizuka, R., 1984. A biochemical study of cholinergic neurons of the post-mortem brains from the patients with Alzheimer-type dementia. Rinsho Shinkeigaku 24, 1128–1135.

Atack, J.R., Perry, E.K., Bonham, J.R., Perry, R.H., 1987. Molecular forms of acetylcholinesterase and butyrylcholinesterase in human plasma and cerebrospinal fluid. J. Neurochem. 48, 1845–1850.

Bateman, R.J., Xiong, C., Benzinger, T.L., Fagan, A.M., Goate, A., Fox, N.C., Marcus, D.S., Cairns, N.J., Xie, X., Blazey, T.M., Holtzman, D.M., Santacruz, A., Buckles, V., Oliver, A., Moulder, K., Aisen, P.S., Ghetti, B., Klunk, W.E., McDade, E., Martins, R.N., Masters, C.L., Mayeux, R., Ringman, J.M., Rossor, M.N., Schofield, P.R., Sperling, R.A., Salloway, S., Morris, J.C., Network, D.I.A., 2012. Clinical and biomarker changes in dominantly inherited Alzheimer's disease. N. Engl. J. Med. 367, 795–804.

Berres, M., Monsch, A.U., Bernasconi, F., Thalmann, B., Stähelin, H.B., 2000. Normal ranges of neuropsychological tests for the diagnosis of Alzheimer's disease. Stud Health Technol Inform 77, 195–199.

Bohnen, N.I., Grothe, M.J., Ray, N.J., Müller, M.L.T.M., Teipel, S.J., 2018. Recent advances in cholinergic imaging and cognitive decline-revisiting the cholinergic hypothesis of dementia. Curr Geriatr Rep 7, 1–11.

Cummings, J.L., Morstorf, T., Zhong, K., 2014. Alzheimer's disease drug-development pipeline: few candidates, frequent failures. Alzheimers Res. Ther. 6, 37.

Daerr, S., Brendel, M., Zach, C., Mille, E., Schilling, D., Zacherl, M.J., Bürger, K., Danek, A., Pogarell, O., Schildan, A., Patt, M., Barthel, H., Sabri, O., Bartenstein, P., Rominger, A., 2017. Evaluation of early-phase. Neuroimage Clin 14, 77–86.

Dale, A.M., Fischl, B., Sereno, M.I., 1999. Cortical surface-based analysis. I. segmentation and surface reconstruction. Neuroimage 9, 179–194.

Fischl, B., Salat, D.H., Busa, E., Albert, M., Dieterich, M., Haselgrove, C., van der Kouwe, A., Killiany, R., Kennedy, D., Klaveness, S., Montillo, A., Makris, N., Rosen, B., Dale, A.M., 2002. Whole brain segmentation: automated labeling of neuroanatomical structures in the human brain. Neuron 33, 341–355.

Fischl, B., Salat, D.H., van der Kouwe, A.J., Makris, N., Ségonne, F., Quinn, B.T., Dale, A.M., 2004. Sequence-independent segmentation of magnetic resonance images. Neuroimage 23 (Suppl. 1), S69–S84.

Forsberg, A., Engler, H., Blomquist, G., Långström, B., Nordberg, A., 2012. The use of PIB-PET as a dual pathological and functional biomarker in AD. Biochim. Biophys. Acta 1822, 380–385.

Grothe, M.J., Heinsen, H., Amaro, E., Grinberg, L.T., Teipel, S.J., 2016. Cognitive correlates of basal forebrain atrophy and associated cortical hypometabolism in mild cognitive impairment. Cereb. Cortex 26, 2411–2426.

Haense, C., Kalbe, E., Herholz, K., Hohmann, C., Neumaier, B., Krais, R., Heiss, W.D., 2012. Cholinergic system function and cognition in mild cognitive impairment. Neurobiol. Aging 33, 867–877.

Hammes, J., Leuwer, I., Bischof, G.N., Drzezga, A., van Eimeren, T., 2017. Multimodal correlation of dynamic [^{18}F]-AV-1451 perfusion PET and neuronal hypometabolism in [^{18}F]-FDG PET. Eur. J. Nucl. Med. Mol. Imaging 44, 2249–2256.

Hampel, H., Mesulam, M.M., Cuello, A.C., Farlow, M.R., Giacobini, E., Grossberg, G.T., Khachaturian, A.S., Vergallo, A., Cavedo, E., Snyder, P.J., Khachaturian, Z.S., 2018a. The cholinergic system in the pathophysiology and treatment of Alzheimer's disease. Brain 141, 1917–1933.

Hampel, H., Vergallo, A., Aguilar, L.F., Benda, N., Broich, K., Cuello, A.C., Cummings, J., Dubois, B., Federoff, H.J., Fiandaca, M., Genthon, R., Haberkamp, M., Karran, E., Mapstone, M., Perry, G., Schneider, L.S., Welikovitch, L.A., Woodcock, J., Baldacci, F., Lista, S., (APMI), A.P.M.I, 2018b. Precision pharmacology for Alzheimer's disease. Pharmacol. Res. 130, 331–365.

Helmstaedter, C., Lendt, M., Lux, S., 2001. Verbaler Lern- und Merkfähigkeitstest. Beltz Test GmbH, Göttingen.

Herholz, K., 1995. FDG PET and differential diagnosis of dementia. Alzheimer Dis. Assoc. Disord. 9, 6–16.

Herholz, K., Bauer, B., Wienhard, K., Kracht, L., Mielke, R., Lenz, M.O., Strotmann, T., Heiss, W.D., 2000. In-vivo measurements of regional acetylcholine esterase activity in degenerative dementia: comparison with blood flow and glucose metabolism. J. Neural Transm. 107, 1457–1468.

Herzog, H., Langen, K.J., Weirich, C., Rota Kops, E., Kaffanke, J., Tellmann, L., Scheins, J., Neuner, I., Stoffels, G., Fischer, K., Caldeira, L., Coenen, H.H., Shah, N.J., 2011. High

resolution Brainpet combined with simultaneous MRI. Nuklearmedizin 50, 74–82.

Hindmarch, I., Lehfeld, H., de Jongh, P., Erzigkeit, H., 1998. The Bayer activities of daily living scale (B-ADL). Dement. Geriatr. Cogn. Disord. 9 (Suppl. 2), 20–26.

Horn, W., 1983. L-P-S Leistungsprüfsystem. Hogrefe, Göttingen.

Hsiao, I.T., Huang, C.C., Hsieh, C.J., Hsu, W.C., Wey, S.P., Yen, T.C., Kung, M.P., Lin, K.J., 2012. Correlation of early-phase 18F-florbetapir (AV-45/Amyvid) PET images to FDG images: preliminary studies. Eur. J. Nucl. Med. Mol. Imaging 39, 613–620.

Jack, C.R., Knopman, D.S., Jagust, W.J., Shaw, L.M., Aisen, P.S., Weiner, M.W., Petersen, R.C., Trojanowski, J.Q., 2010. Hypothetical model of dynamic biomarkers of the Alzheimer's pathological cascade. Lancet Neurol. 9, 119–128.

Jenkinson, M., Smith, S., 2001. A global optimisation method for robust affine registration of brain images. Med. Image Anal. 5, 143–156.

Jenkinson, M., Bannister, P., Brady, M., Smith, S., 2002. Improved optimization for the robust and accurate linear registration and motion correction of brain images. Neuroimage 17, 825–841.

Kessler, J., Markowitsch, H.J., Denzler, P.E., 1990. Mini-Mental-Status-Test (Dt. Fassung). Hogrefe, Göttingen.

Knopman, D.S., Jack, C.R., Wiste, H.J., Weigand, S.D., Vemuri, P., Lowe, V., Kantarci, K., Gunter, J.L., Senjem, M.L., Ivnik, R.J., Roberts, R.O., Boeve, B.F., Petersen, R.C., 2012. Short-term clinical outcomes for stages of NIA-AA preclinical Alzheimer disease. Neurology 78, 1576–1582.

Liu, A.K., Chang, R.C., Pearce, R.K., Gentleman, S.M., 2015. Nucleus basalis of meynert revisited: anatomy, history and differential involvement in Alzheimer's and Parkinson's disease. Acta Neuropathol. 129, 527–540.

Makris, N., Goldstein, J.M., Kennedy, D., Hodge, S.M., Caviness, V.S., Faraone, S.V., Tsuang, M.T., Seidman, L.J., 2006. Decreased volume of left and total anterior insular lobule in schizophrenia. Schizophr. Res. 83, 155–171.

Mazziotta, J., Toga, A., Evans, A., Fox, P., Lancaster, J., Zilles, K., Woods, R., Paus, T., Simpson, G., Pike, B., Holmes, C., Collins, L., Thompson, P., MacDonald, D., Iacoboni, M., Schormann, T., Amunts, K., Palomero-Gallagher, N., Geyer, S., Parsons, L., Narr, K., Kabani, N., Le Goualher, G., Boomsma, D., Cannon, T., Kawashima, R., Mazoyer, B., 2001. A probabilistic atlas and reference system for the human brain: International Consortium for Brain Mapping (ICBM). Philos. Trans. R. Soc. Lond. Ser. B Biol. Sci. 356, 1293–1322.

Mielke, R., Pietrzyk, U., Jacobs, A., Fink, G.R., Ichimiya, A., Kessler, J., Herholz, K., Heiss, W.D., 1994. HMPAO SPET and FDG PET in Alzheimer's disease and vascular dementia: comparison of perfusion and metabolic pattern. Eur. J. Nucl. Med. 21, 1052–1060.

Minoshima, S., Frey, K.A., Koeppe, R.A., Foster, N.L., Kuhl, D.E., 1995. A diagnostic approach in Alzheimer's disease using three-dimensional stereotactic surface projections of fluorine-18-FDG PET. J. Nucl. Med. 36, 1238–1248.

Minoshima, S., Giordani, B., Berent, S., Frey, K.A., Foster, N.L., Kuhl, D.E., 1997. Metabolic reduction in the posterior cingulate cortex in very early Alzheimer's disease. Ann. Neurol. 42, 85–94.

Morbelli, S., Bauckneht, M., Arnaldi, D., Picco, A., Pardini, M., Brugnolo, A., Buschiazzo, A., Pagani, M., Girtler, N., Nieri, A., Chincarini, A., De Carli, F., Sambuceti, G., Nobili, F., 2017. 18F-FDG PET diagnostic and prognostic patterns do not overlap in Alzheimer's disease (AD) patients at the mild cognitive impairment (MCI) stage. Eur. J. Nucl. Med. Mol. Imaging 44, 2073–2083.

Namba, H., Iyo, M., Fukushi, K., Shinotoh, H., Nagatsuka, S., Suhara, T., Sudo, Y., Suzuki, K., Irie, T., 1999. Human cerebral acetylcholinesterase activity measured with positron emission tomography: procedure, normal values and effect of age. Eur. J. Nucl. Med. 26, 135–143.

Nichols, T.E., Holmes, A.P., 2002. Nonparametric permutation tests for functional neuroimaging: a primer with examples. Hum. Brain Mapp. 15, 1–25.

Pagani, M., De Carli, F., Morbelli, S., Öberg, J., Chincarini, A., Frisoni, G.B., Galluzzi, S., Perneczky, R., Drzezga, A., van Berckel, B.N., Ossenkoppele, R., Didic, M., Guedj, E., Brugnolo, A., Picco, A., Arnaldi, D., Ferrara, M., Buschiazzo, A., Sambuceti, G., Nobili, F., 2015. Volume of interest-based [18F]fluorodeoxyglucose PET discriminates MCI converting to Alzheimer's disease from healthy controls. A European Alzheimer's Disease Consortium (EADC) study. Neuroimage Clin 7, 34–42.

Paulson, O.B., Hasselbalch, S.G., Rostrup, E., Knudsen, G.M., Pelligrino, D., 2010. Cerebral blood flow response to functional activation. J. Cereb. Blood Flow Metab. 30, 2–14.

Rey, A., 1964. L'examen clinique en psychologie. Presses Universitaires de France, Paris.

Richter, N., Michel, A., Onur, O.A., Kracht, L., Dietlein, M., Tittgemeyer, M., Neumaier, B., Fink, G.R., Kukolja, J., 2017. White matter lesions and the cholinergic deficit in aging and mild cognitive impairment. Neurobiol. Aging 53, 27–35.

Richter, N., Beckers, N., Onur, O.A., Dietlein, M., Tittgemeyer, M., Kracht, L., Neumaier, B., Fink, G.R., Kukolja, J., 2018. Effect of cholinergic treatment depends on cholinergic integrity in early Alzheimer's disease. Brain 141, 903–915.

Rodriguez-Vieitez, E., Leuzy, A., Chiotis, K., Saint-Aubert, L., Wall, A., Nordberg, A., 2017. Comparability of [^{18}F]THK5317 and [^{11}C]PIB blood flow proxy images with [^{18}F]FDG positron emission tomography in Alzheimer's disease. J. Cereb. Blood Flow Metab. 37, 740–749.

Rostomian, A.H., Madison, C., Rabinovici, G.D., Jagust, W.J., 2011. Early 11C-PIB frames and 18F-FDG PET measures are comparable: a study validated in a cohort of AD and FTLD patients. J. Nucl. Med. 52, 173–179.

Sabri, O., Meyer, P.M., Gräf, S., Hesse, S., Wilke, S., Becker, G.A., Rullmann, M., Patt, M., Luthardt, J., Wagenknecht, G., Hoepping, A., Smits, R., Franke, A., Sattler, B., Tiepolt, S., Fischer, S., Deuther-Conrad, W., Hegerl, U., Barthel, H., Schönknecht, P., Brust, P., 2018. Cognitive correlates of α4β2 nicotinic acetylcholine receptors in mild Alzheimer's dementia. Brain 141, 1840–1854.

Schmitt, M., Altstötter-Gleich, C., Hinz, A., Maes, J., Brähler, E., 2006. Normwerte für das Vereinfachte Beck Depressions-Inventar (BDI-V) in der Allgemeinbevölkerung. Diagnostica 51–59.

Schmitz, T.W., Nathan Spreng, R., Initiative, A.s.D.N., 2016. Basal forebrain degeneration precedes and predicts the cortical spread of Alzheimer's pathology. Nat. Commun. 7, 13249.

Schmitz, T.W., Mur, M., Aghourian, M., Bedard, M.A., Spreng, R.N., Initiative, A.s.D.N., 2018. Longitudinal Alzheimer's degeneration reflects the spatial topography of cholinergic basal forebrain projections. Cell Rep. 24, 38–46.

Schretlen, D.J., Bobholz, J.H., Brandt, J., 1996. Development and psychometric properties of the brief test of attention. Clin. Neuropsychol. 10, 80–89.

Shinotoh, H., Namba, H., Fukushi, K., Nagatsuka, S., Tanaka, N., Aotsuka, A., Tanada, S., Irie, T., 2000. Brain acetylcholinesterase activity in Alzheimer disease measured by positron emission tomography. Alzheimer Dis. Assoc. Disord. 14 (Suppl. 1), S114–S118.

Smith, S.M., Nichols, T.E., 2009. Threshold-free cluster enhancement: addressing problems of smoothing, threshold dependence and localisation in cluster inference. Neuroimage 44, 83–98.

Sperling, R.A., Jack, C.R., Aisen, P.S., 2011. Testing the right target and right drug at the right stage. Sci. Transl. Med. 3, 111cm133.

Teipel, S., Drzezga, A., Grothe, M.J., Barthel, H., Chételat, G., Schuff, N., Skudlarski, P., Cavedo, E., Frisoni, G.B., Hoffmann, W., Thyrian, J.R., Fox, C., Minoshima, S., Sabri, O., Fellgiebel, A., 2015. Multimodal imaging in Alzheimer's disease: validity and usefulness for early detection. Lancet Neurol. 14, 1037–1053.

Teipel, S., Grothe, M.J., Initiative, A.s.D.N., 2016. Does posterior cingulate hypometabolism result from disconnection or local pathology across preclinical and clinical stages of Alzheimer's disease? Eur. J. Nucl. Med. Mol. Imaging 43, 526–536.

Tiepolt, S., Hesse, S., Patt, M., Luthardt, J., Schroeter, M.L., Hoffmann, K.T., Weise, D., Gertz, H.J., Sabri, O., Barthel, H., 2016. Early [^{18}F]florbetaben and [^{11}C]PiB PET images are a surrogate biomarker of neuronal injury in Alzheimer's disease. Eur. J. Nucl. Med. Mol. Imaging 43, 1700–1709.

Winkler, A.M., Ridgway, G.R., Webster, M.A., Smith, S.M., Nichols, T.E., 2014. Permutation inference for the general linear model. Neuroimage 92, 381–397.

Wong, C.Y., Thie, J., Gaskill, M., Ponto, R., Hill, J., Tian, H.Y., Balon, H., Wu, D., Fink-Bennett, D., Nagle, C., 2006. A statistical investigation of normal regional intrasubject heterogeneity of brain metabolism and perfusion by F-18 FDG and O-15 H2O PET imaging. BMC Nucl Med 6, 4.

Zundorf, G., Herholz, K., Lercher, M., Wienhard, K., Bauer, B., Weisenbach, S., Weiss, W.D., 2002. PET functional parametric images of acetylcholine esterase activity without blood sampling. In: Senda, M., Kimura, Y., Herscovitch, P. (Eds.), Brain Imaging Using PET. Academic Press, San Diego, pp. 41–46.